



In vitro bioactivity and stem cells attachment of three-dimensionally ordered macroporous bioactive glass incorporating iron oxides

Thanida Charoensuk, Chitnarong Sirisathitkul, Upsorn Boonyang, Innocent J. Macha, Jerran Santos, David Grossin, Besim Ben-Nissan

► To cite this version:

Thanida Charoensuk, Chitnarong Sirisathitkul, Upsorn Boonyang, Innocent J. Macha, Jerran Santos, et al.. In vitro bioactivity and stem cells attachment of three-dimensionally ordered macroporous bioactive glass incorporating iron oxides. *Journal of Non-Crystalline Solids*, 2016, 452, pp.62-73. 10.1016/j.jnoncrysol.2016.08.019 . hal-02419313

HAL Id: hal-02419313

<https://hal.science/hal-02419313>

Submitted on 19 Dec 2019

HAL is a multi-disciplinary open access archive for the deposit and dissemination of scientific research documents, whether they are published or not. The documents may come from teaching and research institutions in France or abroad, or from public or private research centers.

L'archive ouverte pluridisciplinaire **HAL**, est destinée au dépôt et à la diffusion de documents scientifiques de niveau recherche, publiés ou non, émanant des établissements d'enseignement et de recherche français ou étrangers, des laboratoires publics ou privés.





Open Archive Toulouse Archive Ouverte (OATAO)

OATAO is an open access repository that collects the work of Toulouse researchers and makes it freely available over the web where possible

This is an author's version published in: <http://oatao.univ-toulouse.fr/24467>

Official URL: <https://doi.org/10.1016/j.corsci.2016.03.030>

To cite this version:

Nguyen, Anh Son  and Musiani, Marco and Orazem, Mark E. and Pébère, Nadine  and Tribollet, Bernard and Vivier, Vincent *Impedance study of the influence of chromates on the properties of waterborne coatings deposited on 2024 aluminium alloy.* (2016) Corrosion Science, 109. 174-181. ISSN 0010-938X

Any correspondence concerning this service should be sent
to the repository administrator: tech-oatao@listes-diff.inp-toulouse.fr

In vitro bioactivity and stem cells attachment of three-dimensionally ordered macroporous bioactive glass incorporating iron oxides

Thanida Charoensuk^a, Chitnarong Sirisathitkul^{a,*}, Upsorn Boonyang^a, Innocent J. Macha^{b,1}, Jerran Santos^b, David Grossin^c, Besim Ben-Nissan^b

^a Molecular Technology Research Unit, School of Science, Walailak University, Nakhon Si Thammarat, Thailand

^b Advanced Tissue Regeneration & Drug Delivery Group, School of Life Sciences, University of Technology Sydney, NSW, Australia

^c CIRIMAT Carnot Institute, University of Toulouse, UMR, France

ARTICLE INFO

Keywords:

Magnetic bioactive glass
Mesopore
Macropore
In vitro bioactivity
Stem cells attachment

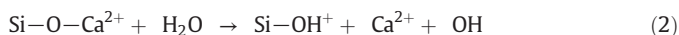
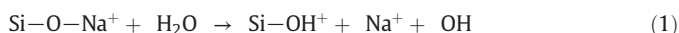
ABSTRACT

Three dimensionally ordered macroporous bioactive SiO₂ CaO Na₂O P₂O₅ glass (3DOM BG) is synthesized by using the sol gel method. After an *in vitro* test in simulated body fluid (SBF), the hydroxyapatite (HAp) crystalline phase is clearly formed on its surface as confirmed by X ray diffractometry (XRD) and Raman spectroscopy. Magnetic 3DOM BG/Fe samples are synthesized by partial substitution of SiO₂ with iron oxide. Whilst the HAp layer is not confirmed, energy dispersive spectroscopy (EDS), Fourier transform infrared spectroscopy (FTIR) and XRD analysis reveal calcium phosphate layer on the surface of 3DOM BG/Fe samples after the SBF soaking. The growth of HAp like layer is slower with increasing iron oxides. The initial mechanism that thought to induce bone formation is reduced due to the replacement of Ca²⁺ with Fe ions in the glass network. The formation of HAp like layer is modified by the sedimentation of Ca and P while the nonmagnetic 3DOM BG forms the calcium phosphate by the ionic exchange following the *Hench mechanism*. The adult human adipose tissue derived stem cells (hADSCs) can be closely attached and well spread on the flat plate of all 3DOM BG/Fe and 3DOM BG. Without detectable cytotoxicity possibly induced by iron oxides, the osteoblast can be grown and proliferated. In addition to these bioactivity and biocompatibility, porous structures can allow their possible use in targeted drug delivery and magnetic properties of 3DOM BG/Fe can essentially be implemented in hyperthermia therapy.

1. Introduction

The bioactivity of bioactive glasses has been proven by either *in vivo* test in physiological environment or *in vitro* test in simulated body fluid (SBF). The *in vitro* test in SBF is internationally accepted valid method to verify the bone bonding ability with the formation of hydroxyl carbonate apatite (HCA) as the bone like layer [1–3]. The refined recipe of conventional SBF was proposed to the Technical Committee ISO/TC150 of International Organization for Standardization in 2003 by Kokubo [1]. Similar compositions and ionic concentrations in human blood plasma and the SBF were also presented [1]. The bone bonding ability of bioactive glasses is determined from the biodegradability, the dissolution rate of its ions, the formation of new bone tissues and the stimulation of osteoblasts when exposed to physiological fluids or SBF. Particularly, the temperature of the *in vitro* testing for HCA formation of bioactive glasses in SBF must be comparable to the body temperature of 37 °C. The mechanisms of bone bonding reported, especially the first 5 reaction stages generally referred to as the *Hench mechanism*, suggestively confirm the glass bioactivity [2–6].

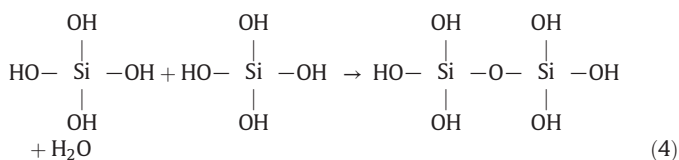
Initially, the network modifications of Na⁺ and Ca²⁺ ions at the interface of glasses are dissolved and replaced by H⁺ from the physiological fluid according to ion exchange reactions in Eqs. (1) and (2).



The increase in pH with increasing OH[−] promotes the breaking of siloxane groups (Si–O–Si). Si(OH)₄ is partly released and silanol groups (Si–OH) are developed at the surface according to Eq. (3).



Owing to the depletion of Na⁺ and Ca²⁺ ions on the surface, the silica rich layer then condenses and repolymerises on the glass surface as follows.



* Corresponding author.

E-mail address: chitnarong.siri@gmail.com (C. Sirisathitkul).

¹ Currently at the University of Dar es Salaam, Dar es Salaam, Tanzania.

Table 1

Chemicals used in the synthesis of 3DOM-BG and 3DOM-BG/Fe.

Sample codes	Composition SiO ₂ -CaO-Na ₂ O-P ₂ O ₅ -Fe (mol%)	P123 (g)	TEOS (mL)	TEP (mL)	1 M NaNO ₃ (mL)	Ca(NO ₃) ₂ ·4H ₂ O (g)	Fe(NO ₃) ₃ ·9H ₂ O (g)	1 M HNO ₃ (mL)	EtOH (mL)
80S/0Fe	80-10-5-5-0	0.667	1.79	0.15	1.00	0.236	–	1.00	2.50
70S/10Fe	70-10-5-5-10	0.581	1.57	0.15	1.00	0.236	0.404	1.00	2.50
60S/20Fe	60-10-5-5-20	0.506	1.34	0.15	1.00	0.236	0.808	1.00	2.50
50S/30Fe	50-10-5-5-30	0.417	1.12	0.15	1.00	0.236	1.212	1.00	2.50

The Ca²⁺ and PO₄³⁻ groups inside of glasses then migrate to the surface at silica rich layer. By incorporating Ca²⁺ and PO₄³⁻ ions in the body fluid, the amorphous CaO P₂O₅ film is formed. The film growth results in the presence of CaO P₂O₅ rich layer on the top surface. The amorphous CaO P₂O₅ rich layer incorporates OH⁻ and/or CO₃²⁻ anions from the surrounding solution. Finally, the HCA is biologically crystallized and new bone tissue is formed by interactions with other biomolecules and cells [2,3].

The continuous reactions after the first 5 stages lead to the implant site for bone tissue repair. The attachment of stem cells, the proliferation and the differentiation of the cells successively occur on the surface of bioactive glasses. The bone mineralization is finally developed with a strong bond to the implant surface [3,7].

The *in vitro* osteogenesis is normally used to assess the potential of the bioactive glasses in bone regeneration. Several human osteoblasts like cells, i.e. MG 63 cells [8], ROS17/2.8 cells [9], bone marrow stromal cells (BMSC) [10], HeLa cells [11], mesenchymal stromal cells (MSC) [12] were studied for the cell adhesive on the surface of bioactive glass samples. These cells were cultured in the mediums (MEM, DMEM, etc.) and supplements (fetal bovine serum, penicillin, streptomycin, etc.) with the controlled temperature at 37 °C in an incubator with simulated human body conditions [13–14]. The biocompatibility in these studies are determined by the cell adhesion ability. The attachment and subsequent proliferation of the osteoblasts like cells have been frequently reported. The morphology and spreading of cells depend on several factors such as the type of cells, the composition of

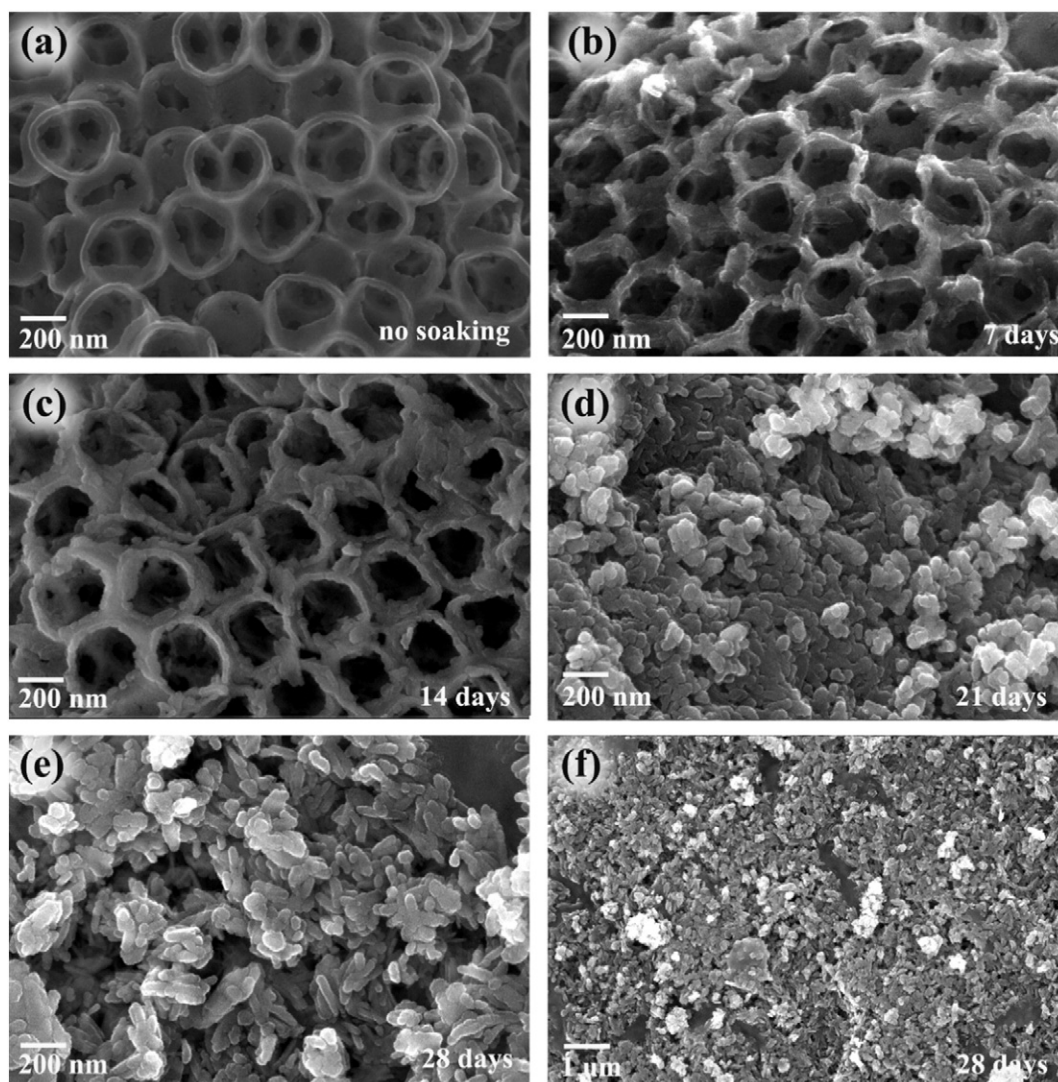


Fig. 1. FESEM images of 80S/0Fe 3DOM-BG (a) before soaking in SBF and after soaking in SBF for (b) 7 days, (c) 14 days, (d) 21 days, (e) 28 days and (f) 28 days shown in a lower magnification.

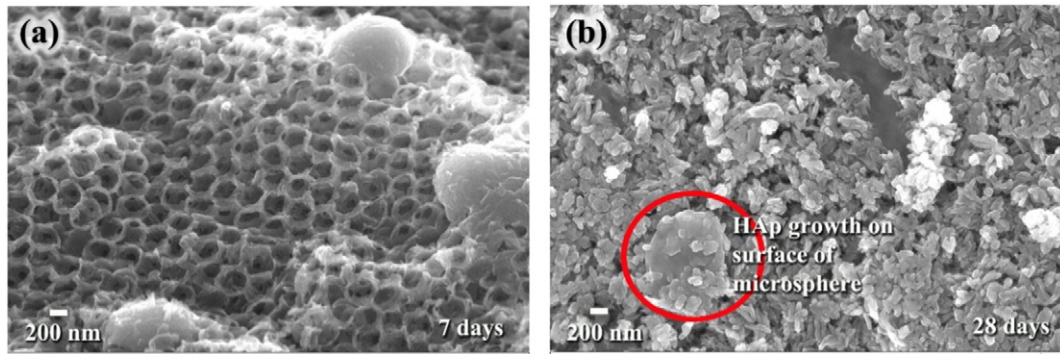


Fig. 2. FESEM images of sample 80S/0Fe showing (a) silica dissolution from microspheres after soaking in SBF for 7 days and (b) HAp crystalline growth on the surface of microsphere after soaking in SBF for 28 days.

bioactive glass samples and the surface micro and macro structure and roughness. The bridging of cells over small pores has been observed. The modifications of porous structures and scaffolds significantly enhance the attachment and proliferation of cell [10]. The interconnected porous structure of the scaffolds supports the vascularization, nutrient as well as allow their use for targeted drug delivery and the tissue growth. By contrast, like any ceramic brittle material its porosity weakens mechanical properties. It has been reported that whereas the doping of MnO_2 and Fe_2O_3 results in the decrease of bioactivity, the cell adhesion and proliferation are facilitated [9]. Since, the hydroxyapatite (HAp) is similar to the major component of human bone, its formation on sample surfaces are believed to enhance cell adhesion and signify the potential for bone tissue regenerations [11,15].

In this study, two glass structures were produced to investigate their bioactivity and biocompatibility. Major aim of the introduction of Fe ions into the structure was their possible use in hyperthermia therapy for cancer patients. The 3DOM structure were obtained in as widely accepted bioactive glass (3DOM BG) and magnetic bioactive glass with the addition of Fe into the structure (3DOM BG/Fe). Both glasses were produced with hierarchical interconnected macropores similar to bone tissues. The HAp formation was monitored to investigate the bioactivity using the SBF *in vitro* test. The stem cells attachment after culturing was examined to verify the bioactivity and biocompatibility. The surfacial changes of 3DOM BG and 3DOM BG/Fe were inspected and compared.

The induction of osteoblast on their surfaces indicated that the materials developed can be used to induce the new bone tissue formation. The superparamagnetic properties were obtained by adding 10 30 mol% $\text{Fe}(\text{NO}_3)_3 \cdot 9\text{H}_2\text{O}$ into SiO_2 CaO Na₂O P₂O₅ glasses which were aimed to be used in hyperthermia therapy.

2. Experimental

2.1. Preparation of 3DOM BG and 3DOM BG/Fe

Based on T. Charoensuk et al. previously published procedure [16], four samples were synthesized with varying compositions of chemicals listed in Table 1. Sample 80S/0Fe was composed of 80SiO₂ 10CaO 5Na₂O 5P₂O₅ and used as a nonmagnetic reference. Three 3DOM BG/Fe samples referred to as 70S/10Fe, 60S/20Fe and 50S/30Fe were respectively prepared with Fe composition of 10, 20 and 30 mol%. Magnetic iron oxide was reduced and incorporated under the reducing carbon environment produced by the thermal decomposition of P123 during the calcination in air atmosphere [11].

2.2. In vitro SBF test

The bioactivity of the obtained samples were examined using r SBF at pH 7.25 following Kokubo method [1]. The grainy 3DOM BG and 3DOM BG/Fe were soaked in SBF. The SBF was daily refreshed and

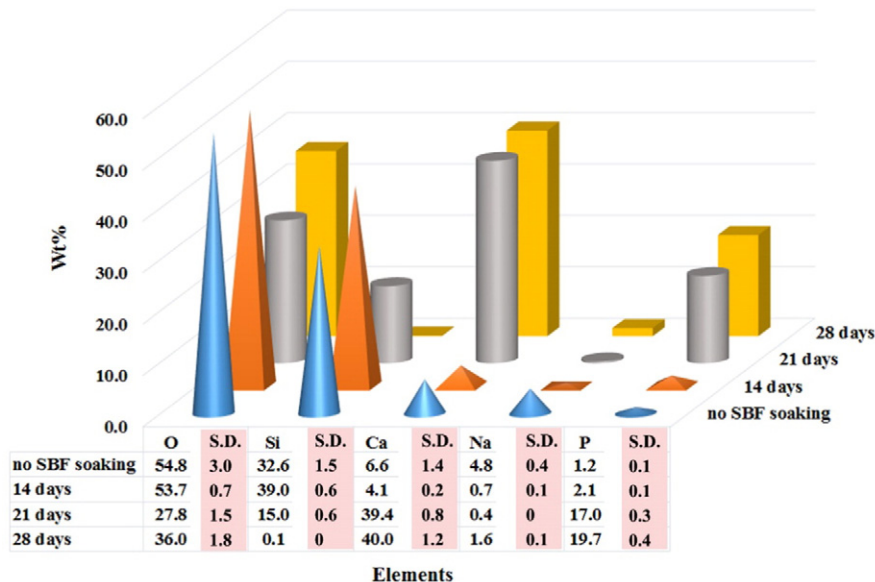


Fig. 3. EDS analysis of elemental composition of 80S/0Fe sample before and after soaking in SBF.

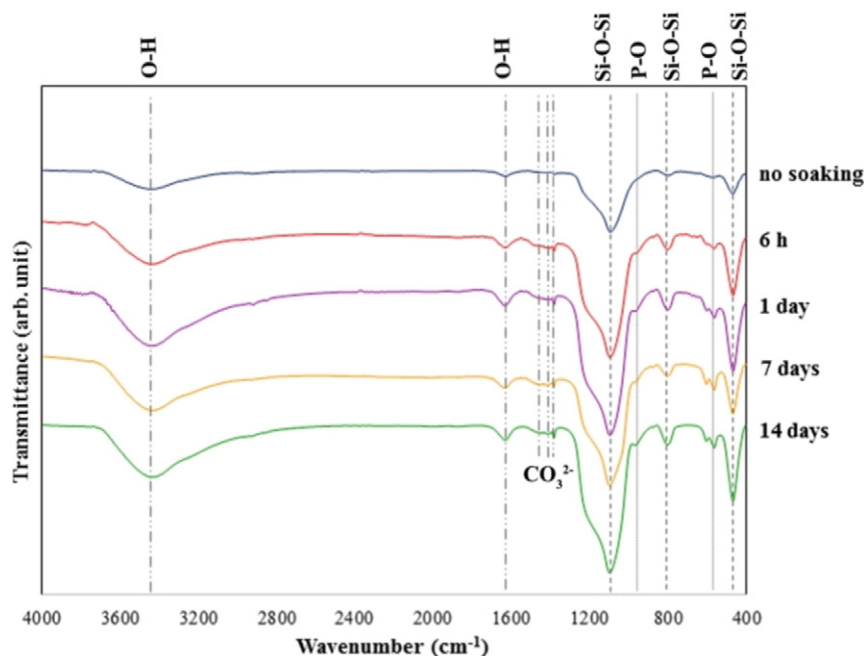


Fig. 4. FTIR spectra of sample 80S/0Fe before and after soaking in SBF.

kept at 37 °C to simulate the *in vivo* situation. The soaking intervals were varied up to 28 days. After soaking, the samples were removed from the SBF, washed 3 times with deionized water and then air dried at the room temperature. The formation of HCA on their surfaces was monitored by field emission scanning electron microscopy (FESEM), energy dispersive spectroscopy (EDS), X ray diffractometry (XRD), Raman and Fourier transform infrared (FTIR) spectroscopy.

2.3. Stem cells attachment

Adult human adipose tissue derived stem cells (hADSCs) tissue culture was conducted under aseptic sterile conditions in a class II laminar flow hood (Clyde Apac BH2000 series). The hADSCs were cultured till sub confluence at 5×10^4 cells/cm² T25 culture flask (Nunc) in Dulbecco's modified Eagle medium (D MEM: Glutmax)/nutrient mixture F12 (Gibco) with 10% fetal bovine serum (FBS: Invitrogen) and incubated at 37 °C at 5% CO₂. Subsequently, cells were passaged and diluted to obtain the seeding density of 10^4 cells/cm². They were placed on the flat plate of 3DOM BG and 3DOM BG/Fe samples for 14 days for the continual growth and adherence test. Non adherent cells that can affect the culture condition were eliminated by replacing the media every 3 days for a normal cellular growth. After the adherence test, media was decanted. The cells were washed in phosphate buffered saline (PBS) and fixed in 4% formalin. They were then washed in distilled water and finally dehydrated for FESEM inspection.

3. Results

3.1. Bioactivity of 3DOM BG

According to FESEM images in Fig. 1, the 3DOM BG (sample 80S/0Fe) was degraded and the HAP like feature was formed by the SBF soaking. Fig. 1(b) indicates deterioration due to the prior release of some soluble silica and Fig. 1(c) demonstrates the initial stage of the crystalline HCA growth. Ultimately, the flake like HCA crystals clearly cover the surface of the sample within 21 days as shown in Fig. 1(d). FESEM also reveals the distortion in the 3DOM structure by interaction between template and precursors due to the addition of Na₂O. The phase separation occurs due to the increase in gel phase resulting in the microspheres on the surface of 3DOM structure as exemplified in

Fig. 2(a). However, the biocompatibility is not affected and the dissoluble efficacy as well as the HCA crystalline growth on the surface of these microspheres is confirmed in the FESEM images.

Fig. 3 compares elemental composition between before and after soaking in SBF for 14, 21 and 28 days. The quantities in wt% of all elements are averaged from over 10 different positions on the sample surface. The Ca and Na are initially decreased after 14 days of SBF soaking but the SBF soaking for 21–28 days leads to large increases in Ca as well as P. For 28 days of SBF soaking, the Ca/P molar ratio is approximately 1.57. The Si is increased after the 14 days of SBF soaking and subsequently decreased until close to zero for 28 days soaking. This EDS analysis confirms the formation of the crystalline HCA phase.

In Fig. 4, the transmittance peaks of FTIR spectra verify the characteristics of bioactive glasses. At the top spectrum, the sample without soaking in SBF exhibits the peaks at 471, 802, 1095 cm⁻¹ and the shoulder at 1095–1220 cm⁻¹ corresponding to the vibration of Si–O–Si bond and the peak at 567 cm⁻¹ correlates to the P–O vibrational peak. In additions, the vibrational peak at 1630 and 3448 cm⁻¹ assigned to O–H bonds indicates the water trapped inside the sample. After the soaking in SBF, the aforementioned vibrational peaks are still observed. The P–O peak at 567 cm⁻¹ split into doublet peak at 565 cm⁻¹ and

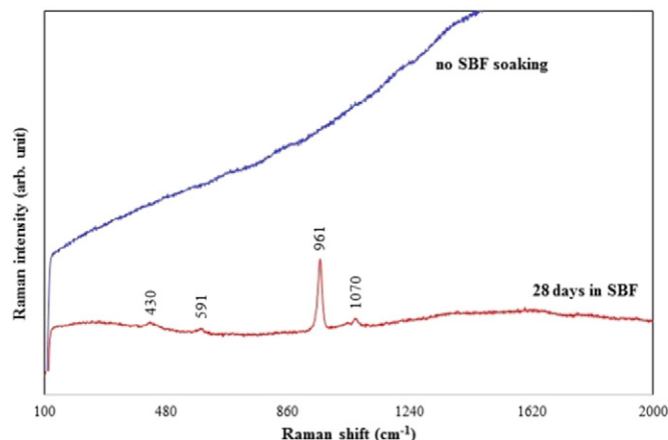


Fig. 5. Raman spectra of sample 80S/0Fe before and after soaking in SBF for 28 days.

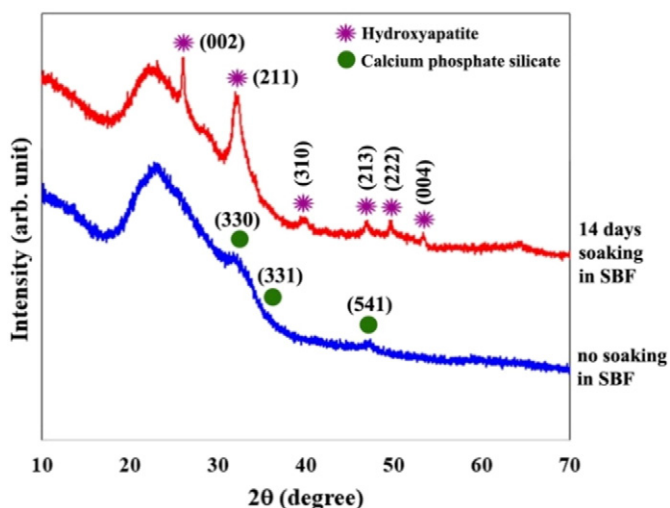


Fig. 6. XRD spectra of sample 80S/0Fe before and after soaking in SBF for 14 days.

602 cm^{-1} and an additional P–O peak can be found at 968 cm^{-1} . In additions, the vibrational peaks around 1380 , 1414 and 1448 cm^{-1} can be assigned to the carbonate group [17–19].

In Fig. 5, the Raman scattering spectrum of 80S/0Fe sample does not exhibit any peak before soaking in SBF since the laser beam in the measurement is only focused on the sample surface. After soaking in SBF for 28 days, the weak peaks at 430 , 591 and 1070 cm^{-1} as well as the sharp and strong peak at 961 cm^{-1} distinctly confirm the growth of HAp crystalline phase. The peaks at 430 and 591 cm^{-1} are related to the O–P–O bending mode. The peaks at 961 and 1070 cm^{-1} correspond to the symmetric stretching mode of P–O bond of PO_4^{3-} and the asymmetric stretching mode of P–O bond [20–21].

Likewise, the XRD patterns shown in Fig. 6 indicate the characteristics of bioactive glasses. A broad reflection around $15-30^\circ$ indicates with amorphous nature of this glassy sample. Before soaking in SBF, additional reflections at 31.7 , 34.5 and 48.4° respectively corresponding to (330), (331) and (541) planes are assigned to calcium phosphate silicate (JCPDS 040 0393). After soaking in SBF for 14 days, the peak positions at 26.0 , 32.0 , 39.8 , 46.9 , 49.8 and 53.3° are assigned to (002), (211), (310), (222), (213) and (004) reflections of HAp, respectively (JCPDS 09 0432).

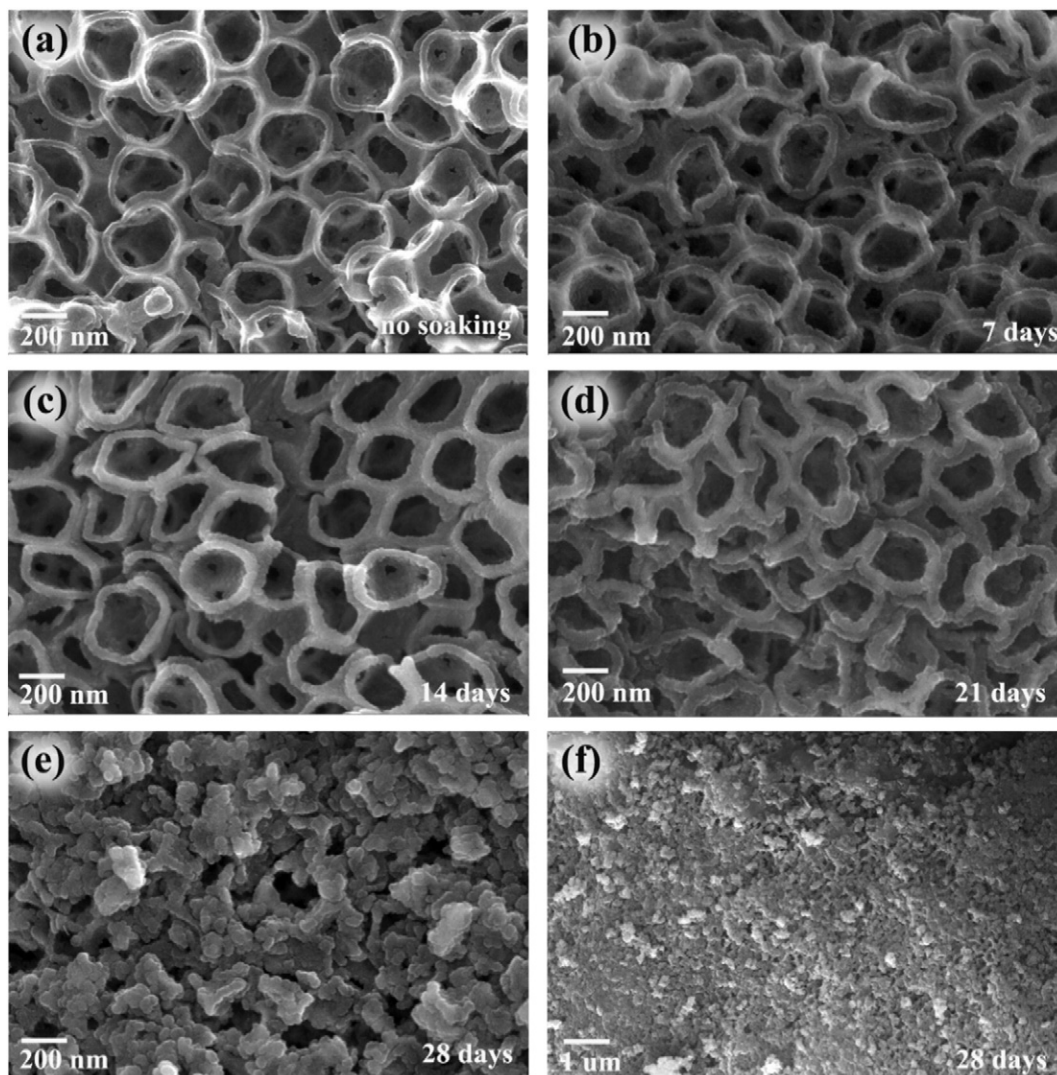


Fig. 7. FESEM images of sample 70S/10Fe (a) before soaking in SBF and after soaking in SBF for (b) 7 days, (c) 14 days, (d) 21 days, (e) 28 days and (f) 28 days shown in a lower magnification.

3.2. Bioactivity of 3DOM BG/Fe

The FESEM images in Figs. 7–9 reveal the surface of 3DOM BG/Fe samples during the bioactivity test. The feature changes after soaking in SBF suggest a different mechanism compared to nonmagnetic 80S/0Fe. A slight change in all 3DOM BG/Fe samples can be observed after soaking in SBF for 7 days. The skeletal walls become thicker after 14 days of soaking in SBF. Obviously, the HAp like feature clearly grows after soaking in SBF for 21 days and most surfaces are covered within 28 days of SBF soaking.

Fig. 10(a) shows the formation microspheres on some outer surface of 50S/30Fe sample similar to those in 80S/0Fe sample. After soaking in SBF, the slightly dissolved silica HAp like features are revealed as in Fig. 10(b). The elemental compositions in the 3DOM BG/Fe before and after the *in vitro* test are analyzed by EDS. The values averaged from over 10 positions on sample 70S/10Fe, 60S/20Fe and 50S/30Fe are respectively compared in Fig. 11(a), (b) and (c). By soaking the samples in SBF, Ca and Na are slightly changed after 14 days and then clearly increased after 21 and 28 days. The Ca/P molar ratio of all samples is only around 0.8 after 28 days and Fe in these 3DOM BG/Fe samples is increased after soaking in SBF.

FTIR spectra for sample 70S/10Fe in Fig. 12(a) show vibrational peaks related to the Si–O–Si bending at 465 cm^{-1} and stretching at 804 cm^{-1} . The P–O vibrational peak is observed at 565 cm^{-1} . According to FTIR spectra of high purity iron oxide nanopowders (>99.5%, US Research Nanomaterials, Inc.), the Fe–O vibrational peaks for Fe_3O_4 at 588 cm^{-1} , $\gamma\text{-Fe}_2\text{O}_3$ at 586 cm^{-1} and $\alpha\text{-Fe}_2\text{O}_3$ at 568 cm^{-1} are close to the P–O peak. Moreover, the Fe–O vibrational peaks of Fe_3O_4 at 1047 and 1094 cm^{-1} as well as $\gamma\text{-Fe}_2\text{O}_3$ at 1063 cm^{-1} are comparable to the Si–O–Si peak. Hence the Fe–O peaks cannot clearly be identified. Unlike sample 80S/0Fe, the splitting of P–O vibrational peak cannot be observed in sample 70S/10Fe after the SBF soaking. The vibrational peak assigned to the carbonate group is observed at 1385 cm^{-1} . In addition, the vibrational peak related to H_2O is located at 1632 and 3450 cm^{-1} .

In Fig. 12(b) and (c), samples 60S/20Fe and 50S/30Fe exhibit vibrational peaks of Si–O–Si, and P–O similar to those of sample 70S/10Fe. The Fe–O peak can also be clearly observed at 698 cm^{-1} . The vibrational peak at around 1730 cm^{-1} corresponded to a carbonyl group and the peaks assigned to the carbonate group at 1385 , 1450 and 1493 cm^{-1} are explicitly found with the increase in Fe composition. After soaking

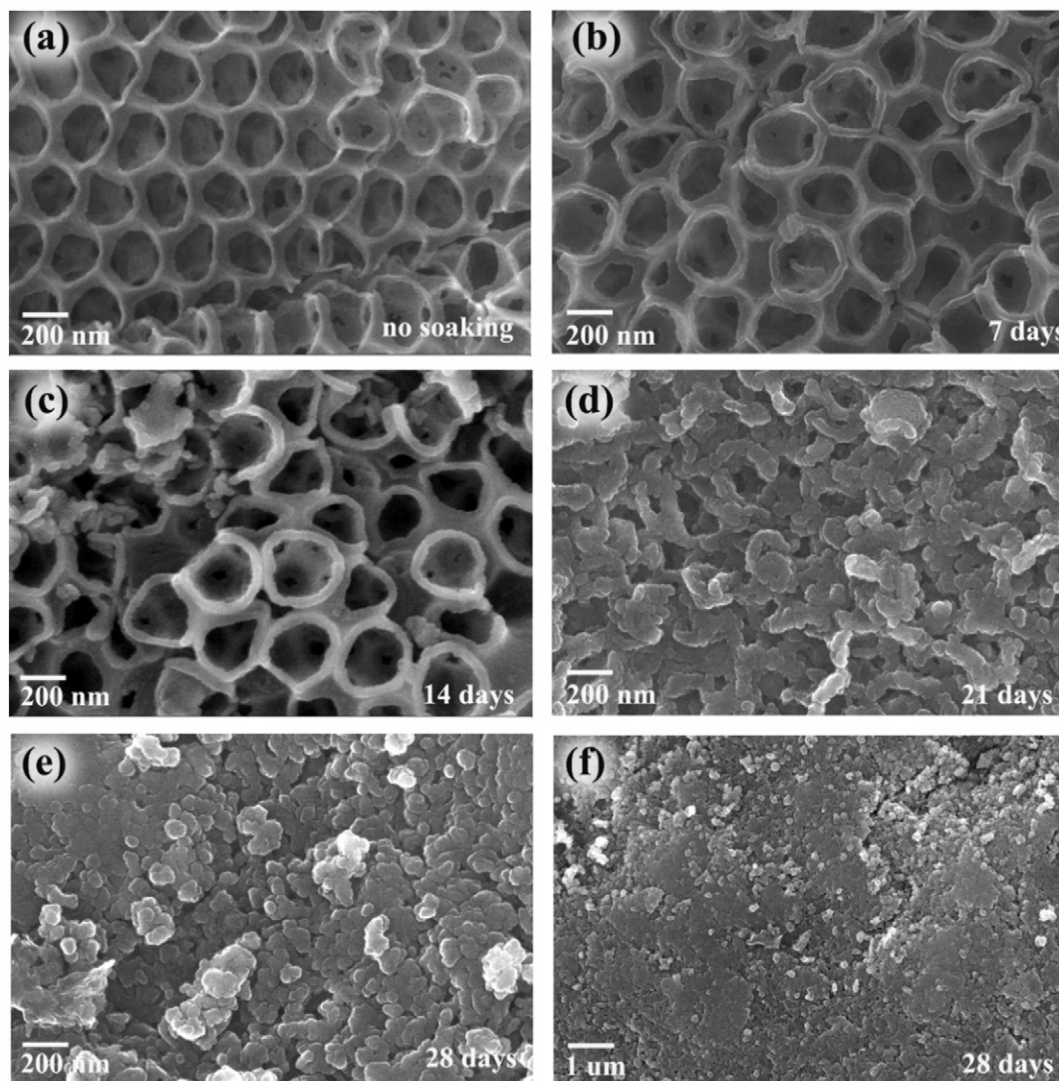


Fig. 8. FESEM images of sample 60S/20Fe (a) before soaking in SBF and after soaking in SBF for (b) 7 days, (c) 14 days, (d) 21 days, (e) 28 days and (f) 28 days shown in a lower magnification.

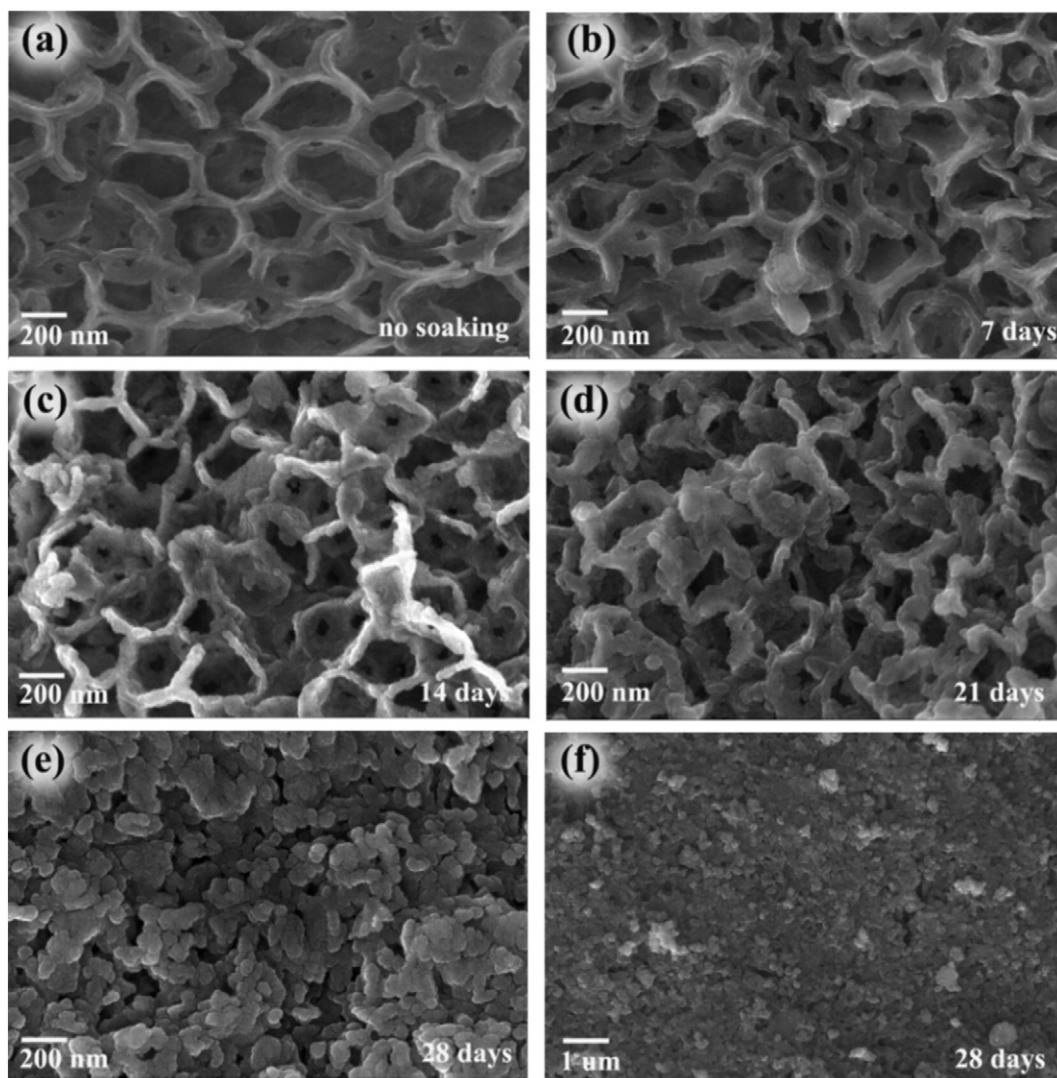


Fig. 9. FESEM images of sample 50S/30Fe (a) before soaking in SBF and after soaking in SBF for (b) 7 days, (c) 14 days, (d) 21 days, (e) 28 days and (f) 28 days shown in a lower magnification.

in SBF, only peak assigned to carbonate at 1385 cm^{-1} remains while other peaks correlated to carbonyl, carbonate and iron oxide gradually disappear. The splitting of P–O peak is not observed. Most vibrational peaks of 3DOM BG/Fe samples tend to shift to lower wavenumbers than those of 3DOM BG (sample 80S/0Fe). This trend also corresponds to the increase in iron oxide concentration.

Before soaking in SBF, four Raman peaks can be observed in Fig. 13(a) for sample 70S/10Fe. The peak at 339 and 702 cm^{-1} can be assigned to $\gamma\text{-Fe}_2\text{O}_3$ [22]. The peak at 965 cm^{-1} is a characteristic of the symmetric stretching of P–O bond. The broad peak at 1380 cm^{-1} can also be attributed to the symmetric stretch of the P=O bond [23]. After soaking in SBF for 28 days, several Raman shifts are observed.

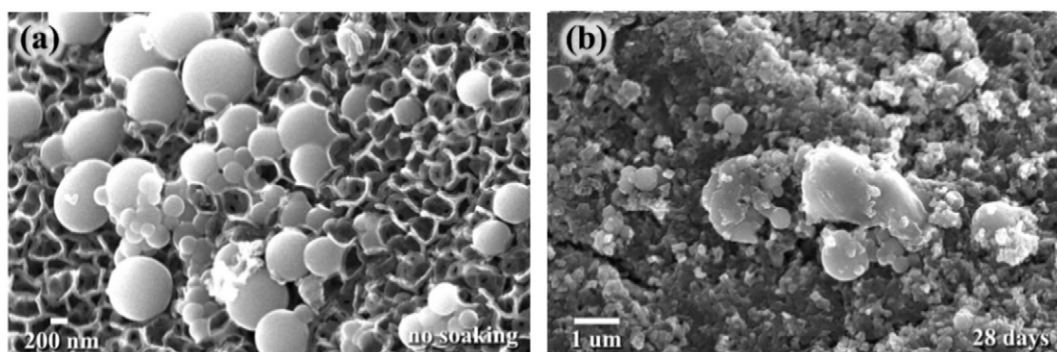


Fig. 10. FESEM images showing microspheres on some surfaces of sample 50S/30Fe (a) before soaking in SBF and (b) after soaking in SBF for 28 days.

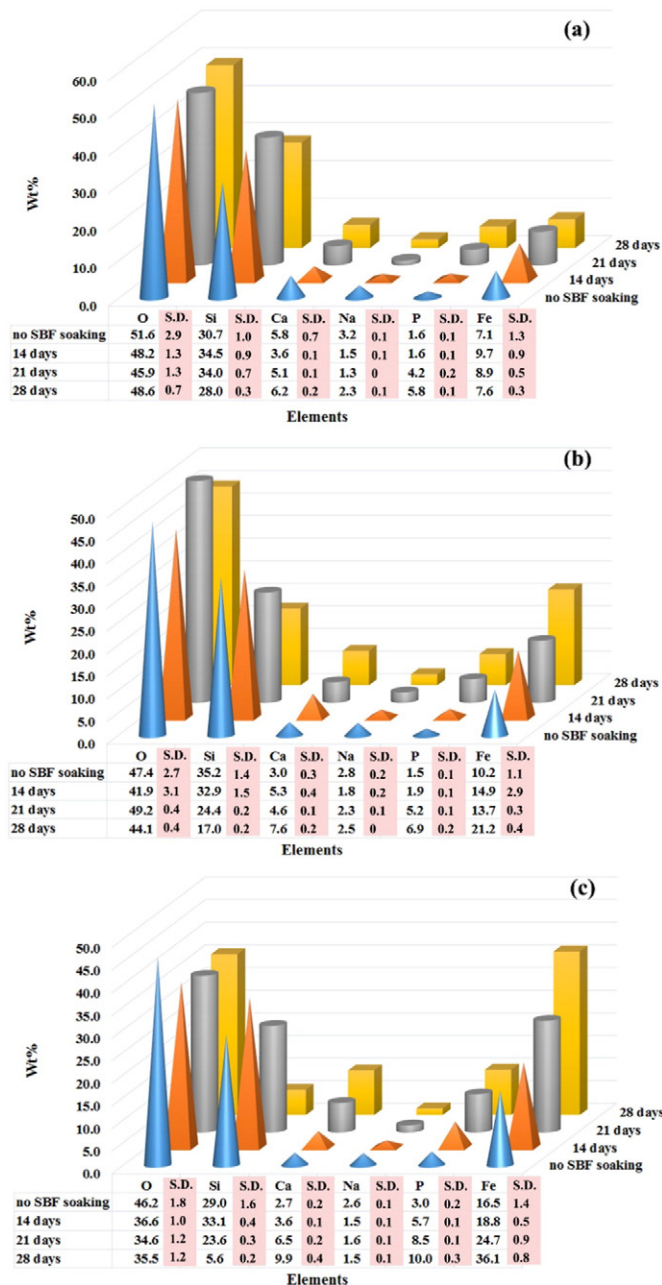


Fig. 11. Comparison of EDS composition analysis of 3DOM-BG/Fe samples before and after soaking in SBF for 14, 21 and 28 days; samples (a) 70S/10Fe, (b) 60S/20Fe and (c) 50S/30Fe.

For iron oxide peaks, the peaks at 228, 293 and 427 cm^{-1} are attributed to α Fe_2O_3 and the peaks at 337, 487, 572 and 671 cm^{-1} correspond to γ Fe_2O_3 [22,24,25]. However, there is a peak shift in the symmetric stretching of P O bond from 965 cm^{-1} to 971 cm^{-1} .

In Fig. 13(b) and (c), the Raman spectra exhibit comparable peaks to those of sample 70S/10Fe. For sample 60S/20Fe before SBF soaking, the peaks at 473 and 691 cm^{-1} correspond to γ Fe_2O_3 and the peak at 973 cm^{-1} is attributed to the P O bond observed. After soaking in SBF for 28 days, the peaks corresponding to γ Fe_2O_3 are found at 330, 487 and 719 cm^{-1} . The peak attributed to the P O bond is shifted to 979 cm^{-1} . For sample 50S/30Fe, the peaks at 334, 479 and 704 cm^{-1} attributed to γ Fe_2O_3 can be observed before SBF soaking. The peaks at 978 and 1380 cm^{-1} are respectively due to P O and P=O bonds. After soaking for 28 days, all peaks are still present with slightly

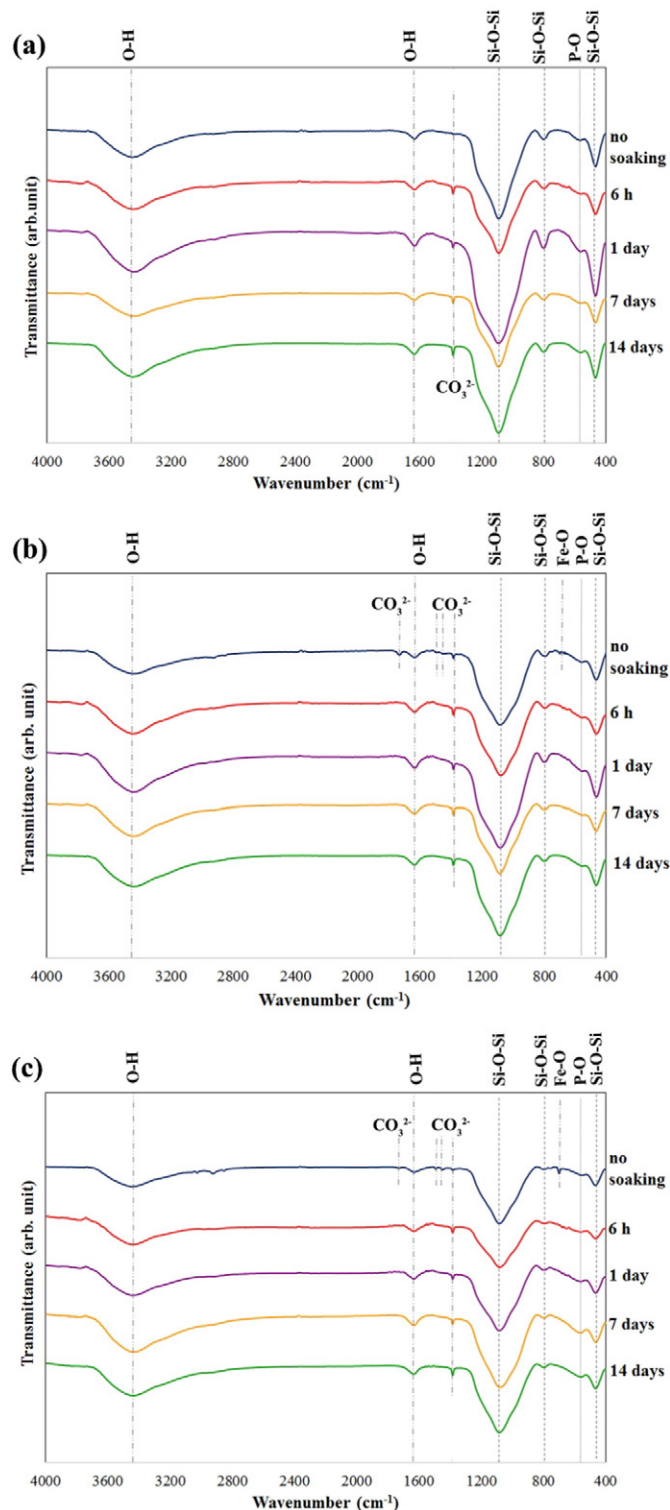


Fig. 12. FTIR spectra of 3DOM-BG/Fe samples before and after soaking in SBF for 6 h–14 days; samples (a) 70S/10Fe, (b) 60S/20Fe and (c) 50S/30Fe.

different intensity. However, the position of P O peak is not shifted for this sample.

The XRD is used to probe the formation of HAP crystalline phase on sample surface. In Fig. 14, the XRD pattern of each 3DOM BG/Fe sample has a broad reflection in the 15–30° regime indicating the amorphous structure of the glass. Sample 70S/10Fe reveals the weakly additional

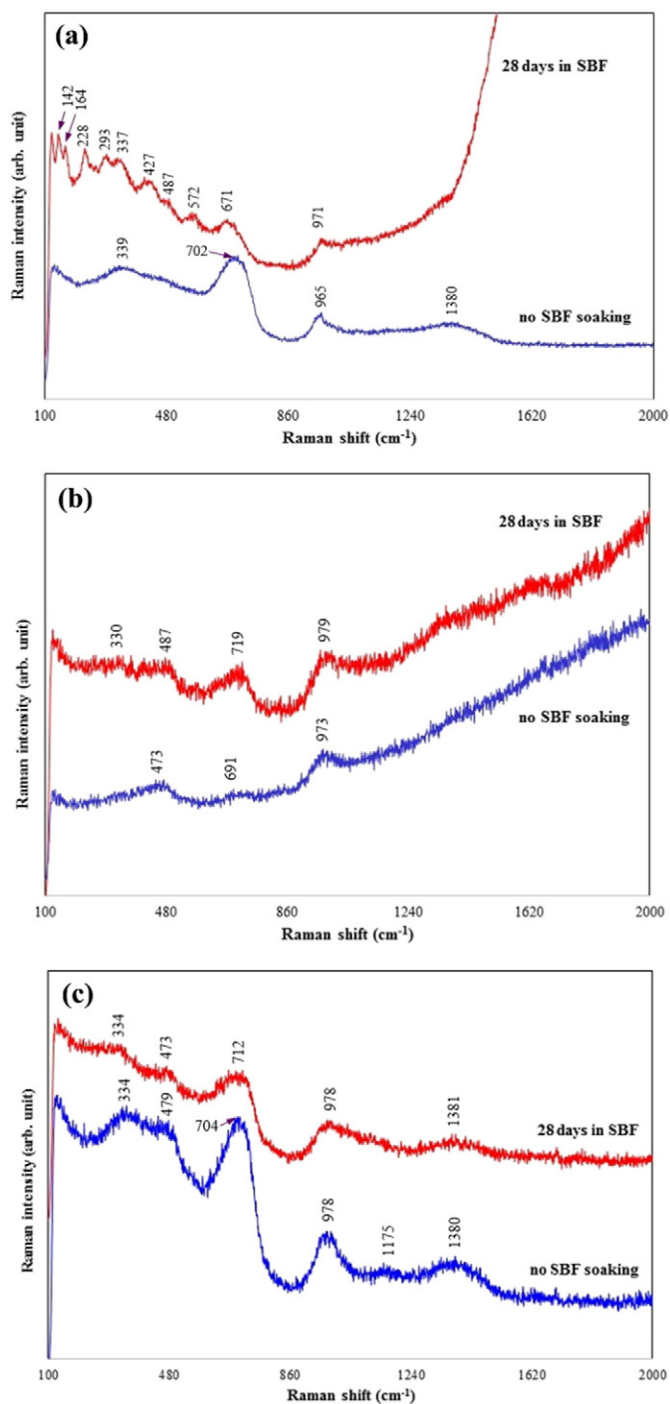


Fig. 13. Raman spectra of 3DOM-BG/Fe samples before and after soaking in SBF for 28 days; samples (a) 70S/10Fe, (b) 60S/20Fe and (c) 50S/30Fe.

reflection at 31.7° assigned to the (330) reflection of calcium phosphate silicate (JCPDS 040 0393). Samples 60S/20Fe and 50S/30Fe exhibit weak and broad characteristic diffraction peaks of γ Fe_2O_3 at 35.6 , 57.2 and 62.7° respectively corresponding to the (311), (511), and (440) reflections (JCPDS 04 0755). However, other peaks assigned to the HAp crystalline phase are not observed after soaking in SBF for 14 days.

3.3. Stem cell attachment

From FESEM images in Fig. 15, the hADSCs are well attached and spread on surface of each sample after the cell culture for 14 days. These cells are over $100\ \mu\text{m}$ in size and mostly triangular in shape.

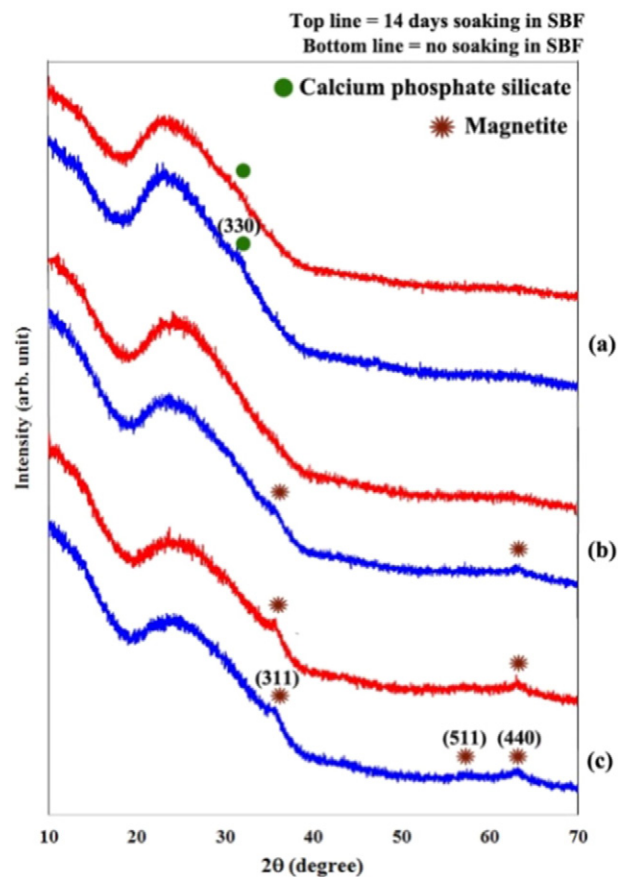


Fig. 14. XRD spectra of 3DOM-BG/Fe samples of (a) 70S/10Fe, (b) 60S/20Fe, and (c) 50S/30Fe before and after soaking in SBF for 14 days.

4. Discussion

4.1. Bioactivity of 3DOM BG

The bioactivity of 3DOM BG is clearly demonstrated in the *in vitro* testing at the controlled temperature of 37°C . When sample 80S/0Fe is soaked in SBF, the first reaction is the ionic exchange between Ca^{2+} and Na^+ linked nonbridging oxygen (NBO) ($\text{Si}-\text{O}-\text{Ca}$ and $\text{Si}-\text{O}-\text{Na}$) with H^+ from solution. The presence of Na^+ in this sample facilitates such exchange. This reaction results in the increase in pH due to the increase in OH^- in the solution. The bridging oxygen (BO) breaking of $\text{Si}-\text{O}-\text{Si}$ bonds is consequently induced by the increase in OH^- and leads to the release of some silica in form of $\text{Si}(\text{OH})_4$ and the formation of $\text{Si}-\text{OH}$ groups at the interface. The SiO_2 rich layer then condenses and repolymerizes on the surface depleted in Ca^{2+} and Na^+ . Subsequently, the amorphous $\text{CaO}-\text{P}_2\text{O}_5$ rich film is formed on the top of the SiO_2 rich layer resulting from the Ca^{2+} and PO_4^{3-} migration to the top. This film is incorporated by Ca^{2+} and PO_4^{3-} from solution leading to the film growth. It follows that the crystalline HCA is formed by the incorporation of OH^- and CO_3^{2-} from the solution. These phenomena involving the first 5 stages of the bone bonding reaction in the *Hench mechanism* [2,6] are explicitly revealed by FESEM images. Conclusively, the Na_2O additive promotes the degradability and bioactivity of the 3DOM BG. In additions, the enhanced reactive surface areas of the 3DOM structure also support the dissolution and resorption abilities resulting in the conversion to the bone like layer [5,26,27].

Although the absolute values are not precisely measured by EDS (it is known to be semi quantitative), the relative amount of each element can be accurately analyzed (as long as standards used) by averaging values over ten different positions on the sample surface. The initial decrease of Ca and Na after SBF soaking indicates the ionic exchange

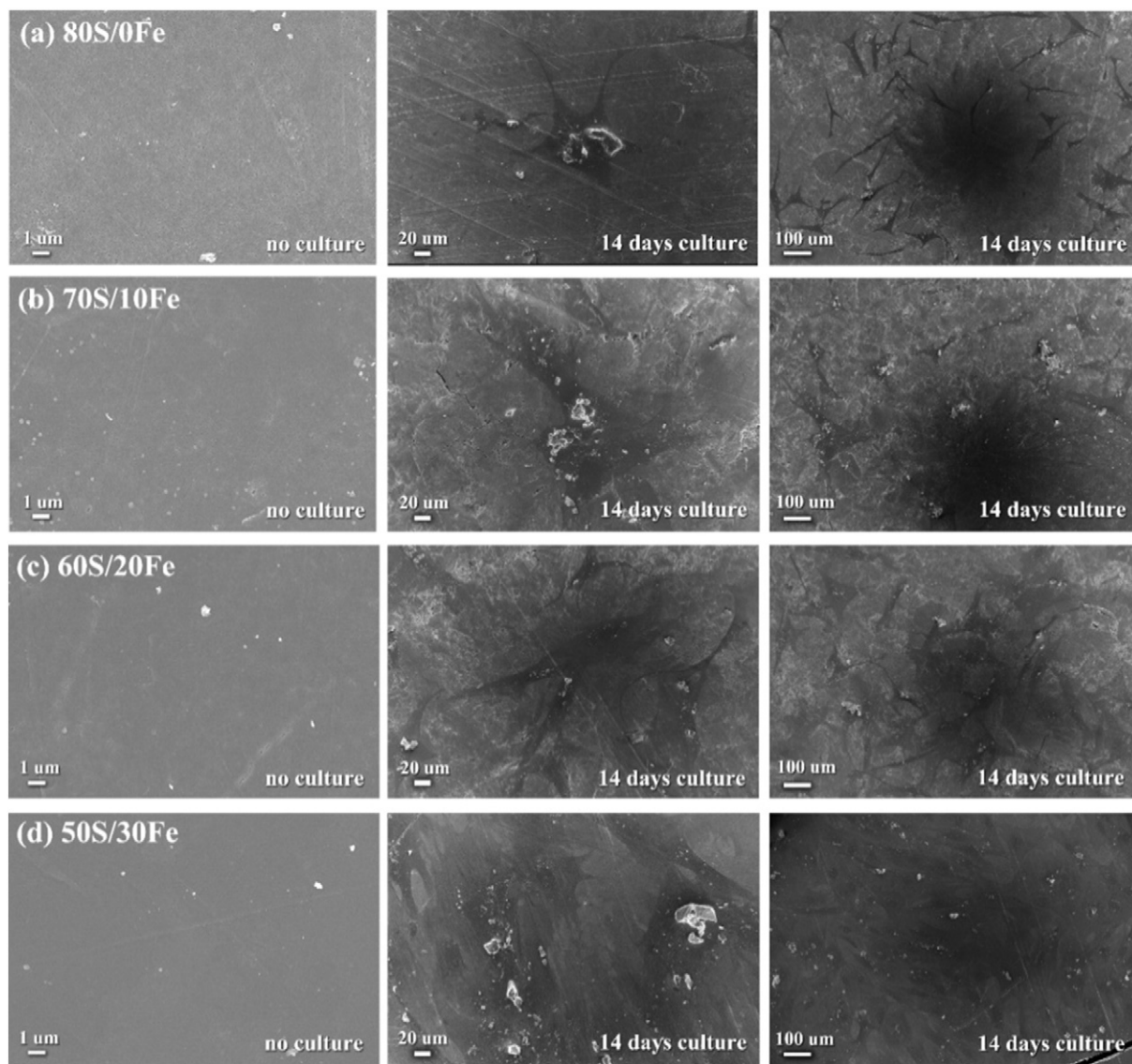


Fig. 15. FESEM images of cells attachment on surface of samples (a) 80S/0Fe, (b) 70S/10Fe, (c) 60S/20Fe and (d) 50S/30Fe after culturing for up to 14 days.

reaction after the soaking. The large increases in Ca as well as P correspond to $\text{CaO P}_2\text{O}_5$ rich films formed at the top of surface and the growth of crystalline HCA. The increase of Si after the 14 days of SBF soaking may involve the formation of SiO_2 rich layer. The subsequent decrease implies the formation of $\text{CaO P}_2\text{O}_5$ rich films on the surface. The minimum Si in the case of 28 days of SBF soaking indicates the fully covered surface by $\text{CaO P}_2\text{O}_5$ rich films and/or HCA. After 28 days of SBF soaking, the Ca/P molar ratio of samples is similar to the 1.0–2.0 range of the value present in human body [28,29]. The characteristic bonds of glass are revealed with the Si–O–Si and P–O vibrational peaks in FTIR spectra. The presence of amorphous phosphate groups confirms the HAp formation after the *in vitro* SBF test. The vibrational peaks assigned to carbonate group also indicate the formation of crystallized HCA [30,31]. In additions, the Raman shift and XRD spectra clearly confirm the bioactivity of 3DOM BG.

4.2. Bioactivity of 3DOM BG/Fe

FESEM images demonstrate the HAp formation is apparently reduced with the increase in Fe concentration. The first stage of *Hench mechanism* involving the ion exchange may be disrupted. The Fe is incorporated in 3DOM BG/Fe samples at the expense of Ca [32]. The

release of Ca^{2+} from 3DOM BG/Fe surface which induces the silica dissolution is decreased. However, the feature resembled HAp crystalline phase is formed on the surface by the agglomeration of Ca and P from the SBF. Although the microspheres disrupt some part of 3DOM structure, they do not affect the bioactivity of 3DOM BG/Fe samples.

After the SBF soaking, the changes in all elements observed by EDS can be explained according to the *Hench mechanism*. Initially, the decreases of Ca and Na signify the first stage of ion exchange. The slight changes of Ca and Na correspond to feature changes previously shown by the FESEM images. Subsequent increases in Si as well as Ca and P are due to the formation of SiO_2 rich layer and $\text{CaO P}_2\text{O}_5$ rich film, respectively. However, the increases in Ca and P are smaller than that of the nonmagnetic 3DOM BG indicating that the presence of Fe disrupts the mechanism of HAp growth on these bioactive glasses. The Ca/P molar ratios are not in range of the value in human body. The presence of Fe reduces the ionic exchange, and hence, a less amount of silica is dissolved. The increases in Ca and P after soaking in SBF for 21 and 28 days are due to the sedimentation or agglomeration of Ca and P on the surface of samples during the process of HAp formation. However, the rate is slow since the Ca/P ratio does not reach the value in human body after 28 days of SBF soaking. So, all 3DOM BG/Fe samples are decidedly less bioactive than the nonmagnetic 3DOM BG. The increase of

Fe after soaking in SBF indicates the minimal release from the surface. This finding suggests that iron oxides will be preserved within the structure when these magnetic bioactive glasses are implemented in hyperthermia treatment.

The Fe–O bonds probably overlap the FTIR vibrational peaks with characteristic peaks of bioactive glass [11,33,34]. After soaking in SBF, the changes in structural bonding occurred and the effect of iron oxide concentration result in the lower wavenumbers of most vibrational peaks. In additions, Raman spectra clearly show the bioactivity of 3DOM BG/Fe. The peak shift corresponding to the symmetric stretching of P–O bond is clearly correlated to the increase in Fe concentration. These peak shifts indicate the increase in average length of P–O bonds [23]. The peak shift of P–O bond, also influenced by the SBF soaking, is decreased by the increase in Fe composition. For the 50S/30Fe sample with the highest concentration of iron oxide, the peak shift due to the SBF soaking does not occur like in other cases. Moreover, the Raman shift is found only for the peak related to γ -Fe₂O₃. The γ -Fe₂O₃ nanocrystals is increasingly formed with increasing amounts of Fe.

Although the *in vitro* bioactivity of 3DOM BG/Fe samples is evident, the HAP phase is not confirmed. The presence of Fe in bioactive glass matrix apparently disrupts the formation of HAP. Nevertheless, the Ca–P layers are grown on 3DOM BG/Fe surfaces as shown in FESEM images and XRD patterns.

4.3. Stem cell attachment

The attachment and well spread of cells on all sample surfaces indicating the good biocompatibility. While the degradability and the HAP crystalline phase formation are important to initiate the bone tissue regeneration, the low biodegradability of 3DOM BG/Fe does not disrupt the cell adhesion. The presence of Fe composition reveals no cytotoxicity. The osteoblast is an indication of the capacity of the growth and proliferation on the 3DOM BG as well as 3DOM BG/Fe samples synthesized in this research.

5. Conclusions

In this study, the initial step of HAP growth according to the *Hench mechanism* leading to the bone bonding on 3DOM BG is clearly shown. The XRD, FTIR and Raman spectra confirm the structure of chemical bonds and functional groups of bioactive glasses corresponding to the HAP formation during the SBF soaking. The *in vitro* test by soaking 3DOM BG/Fe samples in SBF indicates different bioactivity from that of the 3DOM BG. The HAP like layer has a lower growth rate in the case of higher Fe concentration. The EDS indicates that the Ca/P ratio is not close to the value found in human bone even after soaking in SBF for 28 days. However, the well adhesion and spread of hADSCs on the flat plate sample after 14 days of the stem cell culture also confirm the biocompatibility of both 3DOM BG and 3DOM BG/Fe. The inclusion of iron oxide does not lead to cytotoxicity and the osteoblast can be grown and proliferated. The presence of iron oxide with superparamagnetic behavior is useful for hyperthermia therapy owing to the induced heat under the alternating magnetic field. The magnetization is increased with the increase in Fe(NO₃)₃·9H₂O from 10 to 30 mol%. The potential applications of these multifunctional bioactive glasses us to replace, repair and regenerate bone defects especially in the bone cancer therapy.

Acknowledgement

This work is financially supported by Walailak University (Molecular Technology Research Unit grant) and Shell Centennial Education Fund (2013), Shell Companies in Thailand. Dr. D. Grossin, Dr. I. Macha and Prof B. Ben Nissan were supported by the Australian Academy of Science and the European Union's Horizon 2020 research and innovation programme under the Marie Skłodowska Curie grant agreement No 645749.

References

- [1] T. Kokubo, H. Takadama, How useful is SBF in predicting *in vivo* bone bioactivity? *Biomaterials* 27 (2006) 2907–2915.
- [2] L.L. Hench, Bioglass: 10 milestones from concept to commerce, *J. Non-Cryst. Solids* 432 (2016) 2–8.
- [3] L.L. Hench, Chronology of bioactive glass development and clinical applications, *New J. Glass Ceram.* 3 (2013) 67–73.
- [4] G. Kaur, O.P. Pandey, K. Singh, D. Homa, B. Scott, G. Pickrell, A review of bioactive glasses: their structure, properties, fabrication, and apatite formation, *J. Biomed. Mater. Res. A* 102 (2013) 254–274.
- [5] F. Bairo, G. Novajra, V. Miguez-Pacheco, A.R. Boccaccini, C. Vitale-Brovarone, Bioactive glasses: special applications outside the skeletal system, *J. Non-Cryst. Solids* 432 (2016) 15–30.
- [6] P.N. Gunawidjaja, R. Mathew, A.Y.H. Lo, I. Izquierdo-Barba, A. García, D. Arcos, M. Vallet-Regí, M. Edén, Local structures of mesoporous bioactive glasses and their surface alterations *in vitro*: inferences from solid-state nuclear magnetic resonance, *Phil. Trans. R. Soc. A* 370 (2012) 1376–1399.
- [7] L.L. Hench, J.M. Polak, Third-generation biomedical materials, *Science* 295 (2002) 1014–1017.
- [8] M. Peter, N.S. Binulal, S.V. Nair, N. Selvamurugan, H. Tamura, R. Jayakumar, Novel biodegradable chitosan-gelatin/nano-bioactive glass ceramic composite scaffolds for alveolar bone tissue engineering, *Chem. Eng. J.* 158 (2010) 353–361.
- [9] G. Li, S. Feng, D. Zhou, Magnetic bioactive glass ceramic in the system CaO–P₂O₅–SiO₂–MgO–CaF₂–MnO₂–Fe₂O₃ for hyperthermia treatment of bone tumor, *J. Mater. Sci. Mater. Med.* 22 (2011) 2197–2206.
- [10] C. Wu, J. Chang, Mesoporous bioactive glasses: structure characteristics, drug/growth factor delivery and bone regeneration application, *Interface Focus* 2 (2012) 292–306.
- [11] D. Wang, H. Lin, J. Jiang, X. Han, W. Guo, X. Wu, Y. Jin, F. Qu, One-pot synthesis of magnetic, macro/mesoporous bioactive glasses for bone tissue engineering, *Sci. Technol. Adv. Mater.* 14 (2013) 025004.
- [12] M.E. Santocildes-Romero, A. Crawford, P.V. Hatton, R.L. Goodchild, I.M. Reaney, C.A. Miller, The osteogenic response of mesenchymal stromal cells to strontium-substituted bioactive glasses, *J. Tissue Eng. Regen. Med.* 9 (2015) 619–631.
- [13] C. Gao, Y. Deng, P. Feng, Z. Mao, P. Li, B. Yang, J. Deng, Y. Cao, C. Shuai, S. Peng, Current progress in bioactive ceramic scaffolds for bone repair and regeneration, *Int. J. Mol. Sci.* 15 (2014) 4714–4732.
- [14] I.A. Silver, J. Deas, M. Erecinska, Interactions of bioactive glasses with osteoblasts *in vitro*: effects of 45S5 bioglass, and 58S and 77S bioactive glasses on metabolism, intracellular ion concentrations and cell viability, *Biomaterials* 22 (2001) 175–185.
- [15] L.-C. Gerhardt, A.R. Boccaccini, Bioactive glass and glass-ceramic scaffolds for bone tissue engineering, *Materials* 3 (2010) 3867–3910.
- [16] T. Charoensuk, C. Sirisathitkul, W. Tangwatanakul, S. Pinisontorn, U. Boonyang, Magnetic phase transitions in macro/mesoporous bioactive glass by ferric nitrate addition in sol-gel synthesis, *J. Ceram. Sci. Tech.* 7 (2016) 139–144.
- [17] A. Lucas-Giro, F.Z. Mezahi, M. Mami, H. Oudadesse, A. Harabi, M.L. Floch, Sol-gel synthesis of a new composition of bioactive glass in the quaternary system SiO₂–CaO–Na₂O–P₂O₅ comparison with melting method, *J. Non-Cryst. Solids* 357 (2011) 3322–3327.
- [18] G.M. Luz, J.A.F. Mano, Preparation and characterization of bioactive glass nanoparticles prepared by sol-gel for biomedical applications, *Nanotechnology* 22 (2011) 494014.
- [19] L. Radev, V. Hristov, I. Michailova, M.H.V. Fernandes, I.M.M. Salvado, *In vitro* bioactivity of biphasic calcium phosphate silicate glassceramic in CaO–SiO₂–P₂O₅ system, *Process. Appl. Ceram.* 4 (2010) 15–24.
- [20] C.S. Ciobanu, F. Massuyeau, L.V. Constantin, D. Predoi, Structural and physical properties of antibacterial Ag-doped nano-hydroxyapatite synthesized at 100 °C, *Nano-scale Res. Lett.* 6 (2011) 1–8.
- [21] L.M.R. de Vasconcellos, Y.R. Carvalho, R.F. do Prado, L.G.O. de Vasconcellos, M.L. de Alencastro Graça, C.A.A. Cairo, Porous titanium by powder metallurgy for biomedical application: characterization, cell cytotoxicity and *in vivo* tests of osseointegration, *Biomedical Engineering – Technical Applications in Medicine*, Intech 2012, pp. 47–74, <http://dx.doi.org/10.5772/47816>.
- [22] S.J. Oh, D.C. Cook, H.E. Townsend, Characterization of iron oxides commonly formed as corrosion products on steel, *Hyperfine Interact.* 112 (1998) 59–65.
- [23] A. Kiani, J.V. Hanna, S.P. King, G.J. Rees, M.E. Smith, N. Roohpour, V. Salih, J.C. Knowles, Structural characterization and physical properties of P₂O₅–CaO–Na₂O–TiO₂ glasses by Fourier transform infrared, Raman and solid-state magic angle spinning nuclear magnetic resonance spectroscopies, *Acta Biomater.* 8 (2012) 333–340.
- [24] M. Hanesch, Raman spectroscopy of iron oxides and (oxy)hydroxides at low laser power and possible applications in environmental magnetic studies, *Geophys. J. Int.* 117 (2009) 941–948.
- [25] M.A.G. Soler, F. Qu, Raman spectroscopy of iron oxide nanoparticles, in: C.S.S.R. Kumar (Ed.), *Raman Spectroscopy for Nanomaterials Characterization*, Springer-Verlag, Berlin Heidelberg, New York 2012, pp. 379–416.
- [26] S.-W. Choi, Y. Zhang, Y. Xia, Three-dimensional scaffolds for tissue engineering: the importance of uniformity in pore size and structure, *Langmuir* 26 (2010) 19001–19006.
- [27] K. Zhang, N.R. Washburn, C.G. Simon Jr., Cytotoxicity of three-dimensionally ordered macroporous sol-gel bioactive glass (3DOM-BG), *Biomaterials* 26 (2005) 4532–4539.
- [28] E. El-Meliegy, R. van Noort, Glasses and Glass Ceramics for Medical Applications, Springer, New York, 2012.
- [29] A.O. Paiva, M.G. Duarte, M.H.V. Fernandes, M.H. Gil, N.G. Costa, *In vitro* studies of bioactive glass/polyhydroxybutyrate composites, *Mater. Res.* 9 (2006) 417–423.

- [30] L.A. Adams, E.R. Essien, R.O. Shaibu, A. Oki, Sol-gel synthesis of $\text{SiO}_2\text{--CaO--Na}_2\text{O--P}_2\text{O}_5$ bioactive glass ceramic from sodium metasilicate, *New J. Glass Ceram.* 3 (2013) 11–15.
- [31] G. Lutisanova, M.T. Palou, J. Kozankova, Comparison of bioactivity *in vitro* of glass and glass ceramic materials during soaking in SBF and DMEM medium, *Ceramics-Silikáty* 55 (2011) 199–207.
- [32] C. Wu, W. Fan, Y. Zhu, M. Gelinsky, J. Chang, G. Cuniberti, V. Albrecht, T. Friis, Y. Xiao, Multifunctional magnetic mesoporous bioactive glass scaffolds with a hierarchical pore structure, *Acta Biomater.* 7 (2011) 3563–3572.
- [33] J. Liu, Y. Cai, Y. Deng, Z. Sun, D. Gu, B. Tu, D. Zhao, Magnetic 3-D ordered macroporous silica templated from binary colloidal crystals and its application for effective removal of microcystin, *Microporous Mesoporous Mater.* 130 (2010) 26–31.
- [34] P. Tartaj, M.d.P. Morales, S. Veintemillas-Verdaguer, T. Gonzalez-Carreno, C.J. Serna, The preparation of magnetic nanoparticles for applications in biomedicine, *J. Phys. D. Appl. Phys.* 36 (2003) R182–R197.